Self-Monitoring and Self-Delivery of Photosensitizer-Doped Nanoparticles for Highly Effective Combination Cancer Therapy *in Vitro* and *in Vivo*

Jinfeng Zhang,[†,●] Yu-Chuan Liang,[▽,●] Xudong Lin,[‡] Xiaoyue Zhu,[†] Li Yan,[†] Shengliang Li,[∥] Xia Yang,[†] Guangyu Zhu,[⊥] Andrey L. Rogach,[§] Peter K. N. Yu,[§] Peng Shi,[‡] Lung-Chen Tu,[#,◆] Chia-Ching Chang,[*,#] Xiaohong Zhang,[*,¶] Xianfeng Chen,[○] Wenjun Zhang,[†] and Chun-Sing Lee[*,†]

[†]Center of Super-Diamond and Advanced Films (COSDAF) & Department of Physics and Materials Science, [‡]Department of Mechanical and Biomedical Engineering, [§]Department of Physics and Materials Science, [⊥]Department of Biology and Chemistry, City University of Hong Kong, 83 Tat Chee Avenue, Kowloon, Hong Kong SAR 999077, P. R. China, [¶]Institute of Functional Nano & Soft Materials (FUNSOM), Jiangsu Key Laboratory for Carbon-Based Functional Materials & Devices, Soochow University, Suzhou, Jiangsu 215123, P. R. China, [∥]Institute of Chemistry, Chinese Academy of Sciences, Beijing 100190, P. R. China, [▽]Agricultural Biotechnology Research Center, Academia Sinica, Taipei, 115, Taiwan, [◆]Department of Plastic Surgery, Mackay Memorial Hospital, Taipei, 10449, Taiwan, [#]Department of Biological Science and Technology, National Chiao Tung University, Hsinchu, Taiwan and Institute of Physics, Academia Sinica, Taipei, Taiwan, and [○]School of Chemistry and Forensic Sciences, Faculty of Life Sciences, University of Bradford, Bradford, BD7 1DP, U.K. [●]These authors contributed equally.

ABSTRACT Theranostic nanomedicine is capable of diagnosis, therapy, and monitoring the delivery and distribution of drug molecules and has received growing interest. Herein, a self-monitored and self-delivered photosensitizer-doped FRET nanoparticle (NP) drug delivery system (DDS) is designed for this purpose. During preparation, a donor/acceptor pair of perylene and 5,10,15,20-tetro (4-pyridyl) porphyrin (H_2TPyP) is co-doped into a chemotherapeutic anticancer drug curcumin (Cur) matrix. In the system, Cur works as a chemotherapeutic agent. In the meantime, the green fluorescence of Cur molecules is quenched (OFF) in the form of NPs and can be subsequently recovered (ON) upon release in tumor cells, which enables additional imaging and real-time self-monitoring capabilities. H_2TPyP is employed as a photodynamic therapeutic drug, but it also emits efficient NIR fluorescence for diagnosis via FRET from perylene. By exploiting the emission characteristics of these two emitters, the combinatorial drugs provide a real-time dual-fluorescent imaging/tracking system *in vitro* and *in vivo*, and this has not been reported before in self-delivered DDS which simultaneously shows a high drug loading capacity (77.6%$_{Cur}$). Overall, our carrier-free DDS is able to achieve chemotherapy (Cur), photodynamic therapy (H_2TPyP), and real-time self-monitoring of the release and distribution of the nanomedicine (Cur and H_2TPyP). More importantly, the as-prepared NPs show high cancer therapeutic efficiency both *in vitro* and *in vivo*. We expect that the present real-time self-monitored and self-delivered DDS with multiple-therapeutic and multiple-fluorescent ability will have broad applications in future cancer therapy.

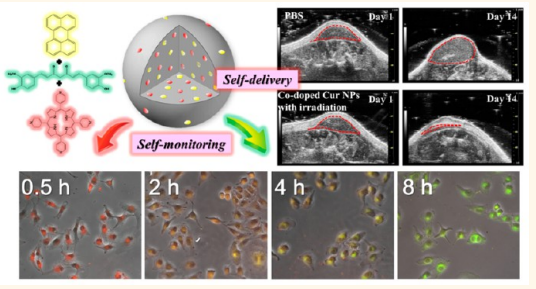

KEYWORDS: self-monitoring · self-delivery · FRET · combination therapy · *in vitro* · *in vivo*

Cancer accounts for millions of deaths annually all over the world.[1] Many types of therapies such as chemotherapy, photodynamic therapy, photothermal therapy, and radiation therapy have been developed for cancer treatment. Chemotherapy is a dominant modality for most cancer cases because of its high efficiency compared to other treatments.[2−6] Photodynamic therapy (PDT) is another promising modality against cancer because of its noninvasiveness and high selectivity.[7−10] In PDT, a photosensitizer (PS) is employed to transfer its absorbed photoenergy to surrounding intracellular oxygen leading to the formation of reactive oxygen species, typically singlet oxygen ($^1O_2$), that consequently induce cell death and necrosis of proximal tissues.[11,12]

Each therapy is effective to some extent, but the outcome of a single therapeutic treatment remains unsatisfactory for completely curing cancer.[13] This deficiency has inspired combinatorial regimens that

* Address correspondence to ccchang01@faculty.nctu.edu.tw, xiaohong_zhang@suda.edu.cn, apcslee@cityu.edu.hk.

Received for review April 27, 2015 and accepted September 21, 2015.

Published online September 21, 2015
10.1021/acsnano.5b02513

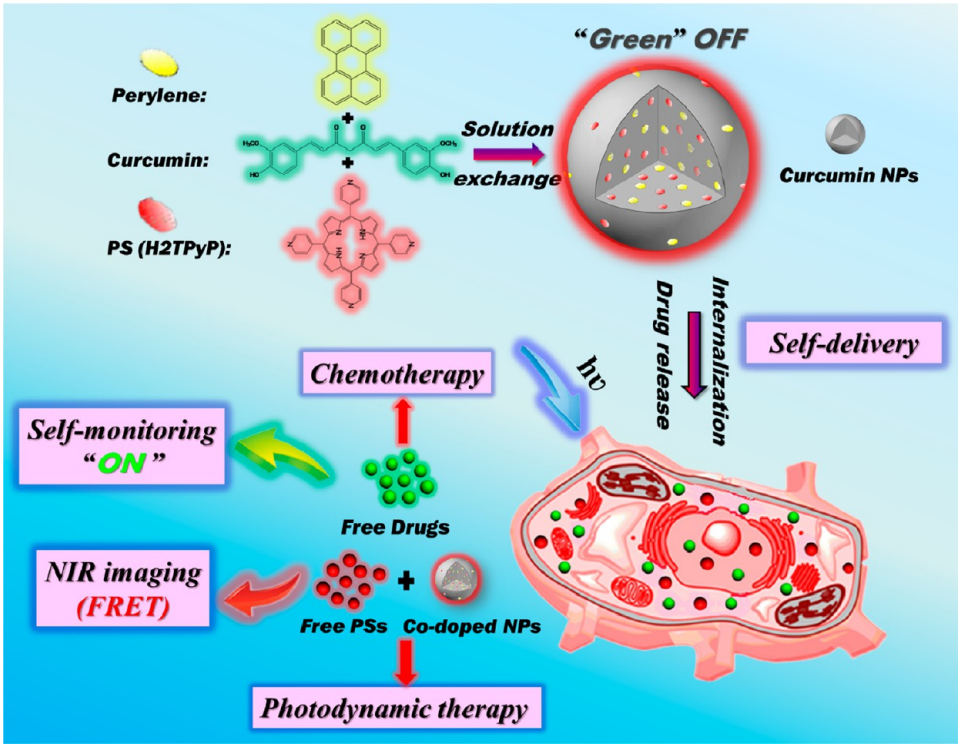

Scheme 1. Schematic illustration on the synthesis of the H_2TPyP (photosensitizer, acceptor) and perylene (donor) co-doped Cur NP and its application for self-delivered and self-monitored chemophotodynamic theranostics. (Cur: chemotherapeutic anticancer drug).

integrate the additive, synergistic, and complementary interactions between different treatments.[14−20] Indeed, researches and clinical applications have demonstrated that combinatorial modalities possess many advantages including improved tumoricidal efficacy, reduced side effects, and retarded drug-resistance.[21−26] Among abundant combination choices, "PDT + chemotherapy" has been shown to be a powerful modality to provide synergistic effects in destructing cancer tissues.[27−32]

So far, an effective and prevalent strategy for achieving combinatorial photochemotherapies is to encapsulate chemotherapeutic drug and photosensitizers into nanostructures of inert carriers to exploit the additional advantages of nanodrugs.[19,20,27−32] However, the drug loading capacities of such systems are comparatively low (typically less than 10%). This significantly reduces effective drug accumulation in targeted tumor areas.[33] In the meantime, the inert carriers may cause undesirable effects.[34,35] For example, repeated administrations of high doses of these excipients can lead to potential systemic toxicity and serious inflammation of internal organs and impose extra burden on patients to excrete the carriers.[36] To overcome these problems, ideally, drugs should be assembled into nanostructures for self-delivery to targeted sites without using any inert carriers.[37−42]

Besides improving therapeutic efficacy with such nanomedicine design, it is also highly desirable to simultaneously achieve diagnosis and real-time monitoring of the release and distribution of drug molecules within the same system. This is typically realized by loading drugs into inert fluorescent NPs or trapping drugs and fluorescent dyes into nonfluorescent NPs.[43−48] However, in both approaches, these inert fluorescent NPs or fluorescent dyes lack therapeutic modality which leads to the issues of low drug loading capacities and potential long-term toxicity. On the other hand, *in situ* self-monitoring of the active drug release in DDSs could be of great benefit, particularly if the reporting signals could be detected in an independent manner based on the intrinsic properties of individual drugs without using the nondrug ingredients' signals. This approach may help in characterizing different therapeutic modalities for the purpose of treatment guidance as well as assessing the response to therapy.

Given these challenges, it is clearly desirable to develop a self-delivered nanodrug without using any excipients but with simultaneous function of combination anticancer therapy, diagnosis, and real-time self-monitoring the release and distribution of different drug molecules. In this work, we report carrier-free PS-doped Förster Resonance Energy Transfer (FRET) NPs to achieve these multifunctions (Scheme 1). In our design, a donor/acceptor pair of perylene and 5,10,15,20-tetro (4-pyridyl) porphyrin (H_2TPyP) is co-doped into a chemotherapeutic anticancer drug curcumin (Cur) matrix (termed as co-doped NPs). The Cur matrix disperses and stabilizes the PSs to prevent their

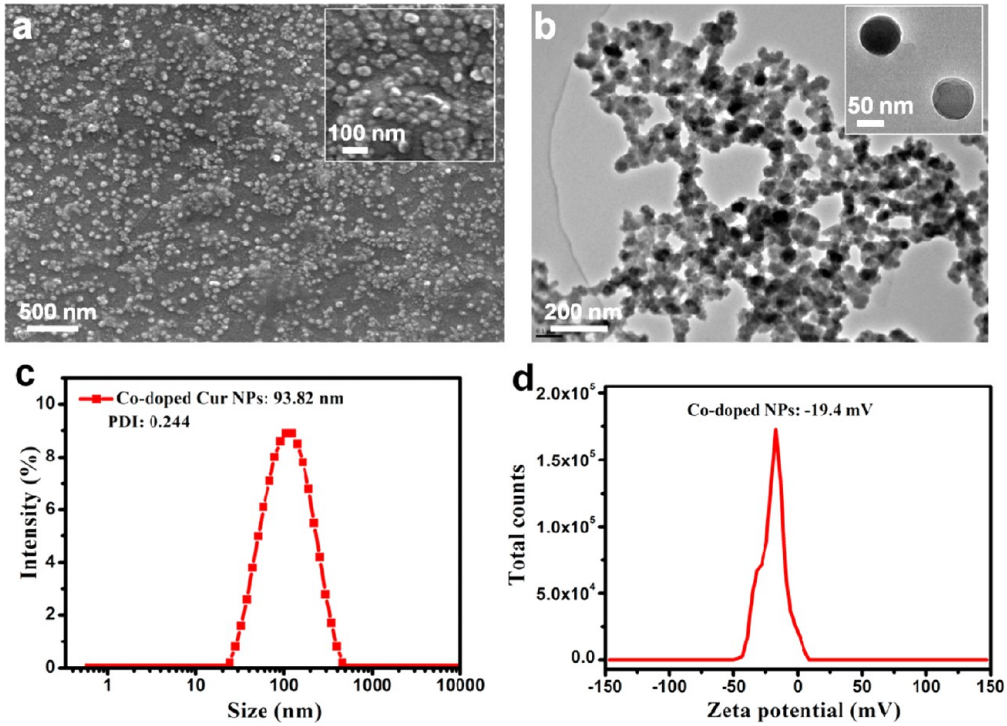

Figure 1. Structural characterization of the co-doped NPs. (a) SEM and (b) TEM images of the co-doped NPs (insets are corresponding SEM and TEM images of higher magnifications). (c) DLS and PDI measurements and (d) zeta potential of the co-doped NPs in aqueous medium.

aggregation and enable their use in an aqueous environment. The green fluorescence of Cur molecules is quenched (OFF) in the form of NPs, but recovered (ON) upon release in tumor cells, enabling real-time self-monitoring of their delivery and release. Meanwhile, H_2TPyP delivers efficient NIR fluorescence for diagnosis as well as generates sufficient $^1O_2$ for PDT via FRET (from perylene) and doping. To demonstrate the concept, herein, we systematically investigated the optical properties, photo- and bioenvironmental stability, and real-time monitoring capacity of the co-doped NPs and tested their *in vitro* and *in vivo* combination therapeutic applications in, respectively, A549 human lung carcinoma cancer cells and on tumor bearing nude mice.

RESULTS AND DISCUSSION

Preparation and Characterization of Co-doped NPs. Figure 1 panels a and b are, respectively, SEM and TEM images of co-doped NPs showing well-defined nanospheres of 80−100 nm in diameter. Dynamic light scattering (DLS) measurement (Figure 1c) gives a hydrodynamic diameter of about 93 nm and a polydispersity index (PDI) of 0.244. The enhanced permeability and retention (EPR) effect is one of the most important features and results of tumor angiogenesis, advantage of which can be taken by nanomedicine to achieve enhanced accumulation in a tumor site.[49] Among different factors, the size of NPs plays the most important role in EPR-based tumor passive targeting. It has been found that NPs with sizes smaller than 200 nm work most effectively in targeting a tumor because particles larger than 200 nm could be cleared from the bloodstream more rapidly by the spleen.[49] The size of the co-doped NPs here is approximate 100 nm which should be suitable for passive targeting via EPR. Furthermore, because of the existence of excess phenolic and enolic hydroxyl groups on Cur, the co-doped NPs appeared to be negatively charged with a zeta potential of around −19.4 mV (Figure 1d).

These NPs are composed of Cur, perylene, and H_2TPyP. Cur is a hydrophobic polyphenol derived from the rhizome of the herb *Curcuma longa* and exhibits a wide range of pharmacological effects including anti-inflammatory, anticancer, and antiangiogenic properties to a broad variety of tumor cell lines.[50] However, its application is hindered by extremely low water solubility and poor bioavailability. Herein, these limitations are addressed by making it in the form of nanomaterials. By reducing the particle size, drug NPs can achieve a high ratio of surface area to volume. Because of the significant increase in the surface area, drug NPs would thus have a greater increased water dispersibility and bioavailability.[51,52]

The action mechanisms of the present nanoplatform are as follows: In the first stage, upon immediate cell-intake, the intact nanoparticles would have no chemotherapeutic effects. They will exhibit strong red fluorescent from H_2TPyP with good PDT via the enhancement effect of FRET from perylene. After

TABLE 1. Composition of the Co-doped NPs

composition	Cur	perylene	H_2TPyP
weight ratio (wt %)	77.6%	22.3%	0.1%

partial release of Cur and H_2TPyP, the released Cur will give green emission and chemotherapeutic effects. The released H_2TPyP will continue to give red emission and PDT effects. However, as the released H_2TPyP and perylene molecules in the cell will have much increased distance well over the effective transfer radius (typical within 10 nm range) of FRET, the FRET effect will no long be significant for the released H_2TPyP. Therefore, in this stage, the released H_2TPyP will behave like free H_2TPyP molecules in solution. Alternately, the undissolved part of the co-doped NPs will continue to give strong red emission and PDT effect via the contribution of the FRET effect. Therefore, in our system, all of the three components make essential and active contribution to the resulting therapeutic effect.

The compositions of the co-doped NPs are listed in Table 1. The weight percentages of Cur, perylene, and H_2TPyP are 77.6%, 22.3%, and 0.1%, respectively. The optimal molar ratio of H_2TPyP in the H_2TPyP−perylene FRET pair is set to be 0.2% to obtain the highest $^1O_2$ yield and the strongest fluorescence according to our previous studies.[53] The co-doped NPs were prepared via the traditional reprecipitation method by rapidly dropping a tetrahydrofuran (THF) solution of Cur, H_2TPyP, and perylene into water under stirring.

An important advantage of the present carrier-free PS-doped FRET NPs is its high drug loading capacity as a combinatorial therapeutic system. As Cur itself constitutes the matrix of the NPs, the average Cur loading efficiency is estimated to be 77.6% by using HPLC and standard absorbance curves (Supporting Information, Figure S1 and S2). Drug loading capacities of most reported nanomaterial-based DDSs for combinatorial therapy are typically below 10% (Table S1). To the best of our knowledge, the drug loading capacity obtained here is the highest among nanomaterial-based DDSs for combinatorial therapy. DDSs with high drug loading would be a potential strategy for future clinical application. This high drug loading capacity addresses various potential adverse effects caused by inert carriers or excipient agents in typical nanomaterial-based DDSs. More importantly, it is more efficient in delivering the active pharmaceutical ingredients by a high-drug-loading DDS per tumor localization event. The total NPs dose needed to deliver a given amount of drugs can thus be extremely reduced. These merits are greatly beneficial to practical clinical translation of nanomaterial-based DDSs in future cancer therapy.

Photophysical Properties of Cur NPs, PS NPs and Co-doped NPs. The present carrier-free theranostic co-doped NPs consist of three optically active materials: H_2TPyP and perylene doped in Cur matrix. The two dopants (H_2TPyP and perylene) are used as a FRET pair. Figure 2a suggests that the emission spectrum of perylene overlaps well with the excitation spectrum of H_2TPyP, which is an essential prerequisite to allow efficient energy transfer. We also measured the change in fluorescence lifetime of H_2TPyP (Figure 2b) and perylene (Figure 2c) upon doping in the Cur matrixes. Accompanying the quenching of perylene fluorescence was a drastically concomitant generation of H_2TPyP emission. The lifetime of perylene NPs is decreased after doping into Cur. In contrast, the lifetime of H_2TPyP increases from 0.041 to 13.67 ns at 655 nm after forming the co-doped NPs. The remarkable opposite changes in fluorescence lifetime are mainly attributed to the FRET effect. Nevertheless, increase in emission lifetime at 655 nm can also due to a reduced aggregation effect or possible electron transfer effects. Further work will be needed to distinguish the relative contributions from these causes.

In the co-doped NPs, the Cur matrix not only hosts and stabilizes the PS (H_2TPyP), but also effectively solves the problem of aggregation and self-quenching of the PS. Cur molecules in solution show a strong green florescent peak at 520 nm. In contrast, Cur solid in the form of NPs displays negligible fluorescence (Figure 2d) due to aggregation induced quenching effect. However, Cur molecules can recover their fluorescence once release from the NPs. Therefore, in addition to hosting the PS, the Cur matrix also plays two other roles of self-delivery and self-monitoring of the drug release with a fluorescence, namely, the "OFF−ON" effect (Figure 2f). Upon entering tumor cells, the co-doped NPs ("OFF"-state) will release Cur molecule ("ON"-state) giving rise to green fluorescence. Meanwhile, in the whole process, H_2TPyP would give red emission and PDT effects both before (with FRET enhancement) and after (without FRET enhancement) releasing.

Figure 2e displays the absorbance and fluorescence spectra of the co-doped NPs. The emission peaks at 655 and 570 nm are attributed to H_2TPyP and perylene, respectively. As expected, no Cur emission (520 nm) appears in the spectrum, indicating the fluorescent state of Cur is "OFF" in the co-doped NPs. This finding is in line with the result shown in Figure 2d. Figure 2f shows photographs of Cur in THF solution and the Cur NPs, the H_2TPyP NPs, and the co-doped NPs (from left to right) in water under room light (upper photo) and UV (lower photo) irradiation. The lower photograph in Figure 2f clearly demonstrates that the original green fluorescence of Cur in solution is quenched upon formation of Cur NPs. The co-doped NPs possess a much stronger red fluorescence upon UV light irradiation when compared to that from the pure H_2TPyP NPs with the same concentration of H_2TPyP in the co-

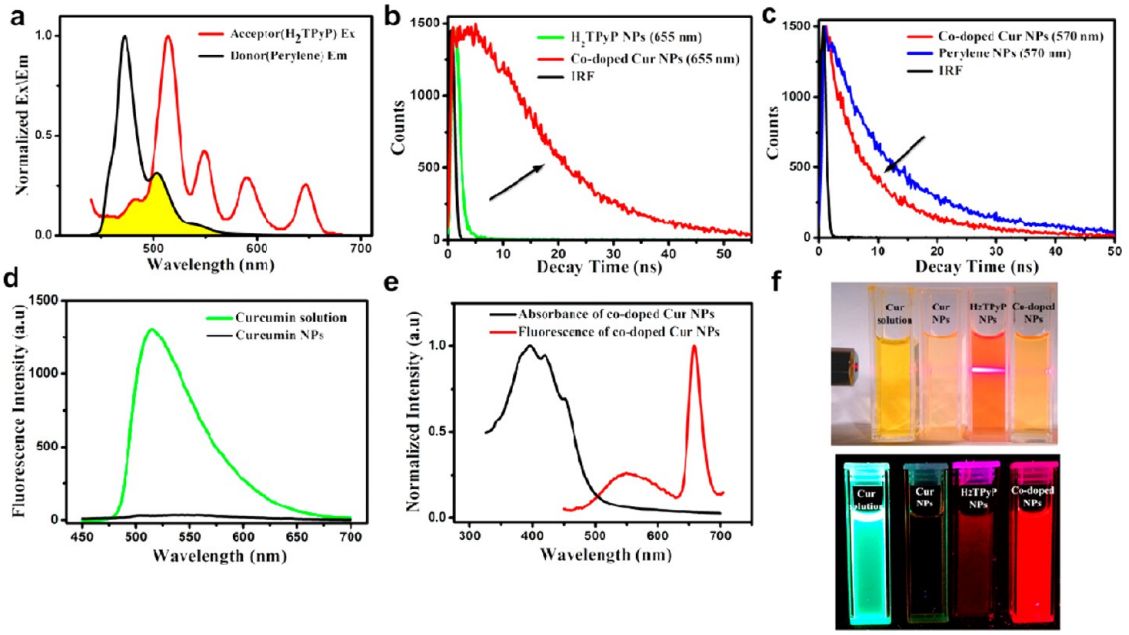

Figure 2. Photophysical properties. (a) Excitation and emission spectra of the H_2TPyP (acceptor) and the perylene (donor). (b) Fluorescence lifetime measurements of H_2TPyP in pure H_2TPyP NPs (green line, 120 μM in water) and co-doped NPs (red line, 120 μM in water) at 655 nm. (c) Fluorescence lifetime measurements of perylene in pure perylene NPs (blue line, 120 μM in water) and co-doped NPs (red line, 120 μM in water) at 570 nm. IRF: instrumental response function. (d) Fluorescence intensity of free Cur in THF and Cur NPs in water. (e) Absorbance and fluorescence spectra of the co-doped NPs. (f) Photographs of the Cur solution, the Cur NPs, the H_2TPyP NPs, and the co-doped NPs under room light (upper photos) and UV light (lower photos). A beam of red laser shines through the samples in the upper photograph to show scattering from the NPs via the Tyndall effect.

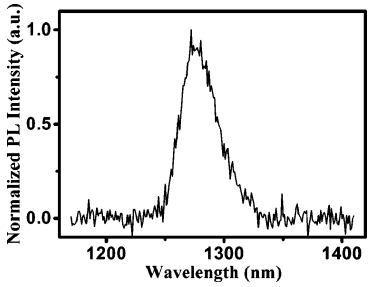

Figure 3. Singlet oxygen phosphorescence emission spectra from the co-doped NPs. The sample was excited at 438 nm, and the experiment was performed in buffered D_2O, which was used because singlet oxygen has a higher phosphorescence quantum efficiency in D_2O than in H_2O.[54]

doped NPs. This indicates that the present co-doping strategy can considerably enhance the fluorescence from H_2TPyP for imaging via the combined effects of doping and FRET (see Figure 2f lower photograph). The fluorescence quantum yield of H_2TPyP in the co-doped NPs dispersed in water is determined to be ~5.57%. It is worth pointing out that carrier-free NPs containing more than one drug with their independent fluorescence at different colors applied to self-monitoring their release have never been reported. The additional OFF−ON switching fluorescence of the Cur matrix further endows the present co-doped NPs with unique multifunctional diagnosis/imaging capabilities.

Generation of Singlet Oxygen ($^1O_2$). To confirm the singlet oxygen generation ability of the co-doped NPs, its photoluminescence spectrum in D_2O was measured (Figure 3). The emission peak around 1272 nm matches well with the $^1O_2$ characteristic phosphorescence emission.[54]

To further monitor the $^1O_2$ generation in the co-doped NPs, we used the disodium salt of 9,10-anthracenedipropionicacid (ADPA) as a sensor, which would be bleached to its endoperoxide in the presence of $^1O_2$.[55] In the experiment, we added ADPA to dispersions of different NPs and recorded the absorption spectra (Figure 4 and Figure S3) of the samples upon continuous irradiation. Figure 4 panels a, b and c are the time-dependent bleaching of ADPA caused by $^1O_2$ generated by the co-doped NPs, the H_2TPyP NPs, and the Cur NPs, respectively. Figure 4d summarizes the variation of the absorbance intensity at 378 nm of different materials as a function of irradiation time. In the sample with the co-doped NPs, the fastest decrease of the absorbance of ADPA indicates the highest singlet oxygen yield from the co-doped NPs. Much less photobleaching of ADPA was observed in the dispersions of the H_2TPyP NPs, the perylene NPs, or the Cur NPs. The much lower $^1O_2$ yield of the H_2TPyP NPs is due to aggregation quenching resulting from $\pi-\pi$ stacking of the planar molecules. The $^1O_2$ quantum yield was measured using a chemical trapping method with ADPA as the trapping agent and Rose Bengal (RB) as the standard photosensitizer ($^1O_2$ quantum yield Φ_{RB} = 0.75 in water). As illustrated in Figure 4d and Figure S4,

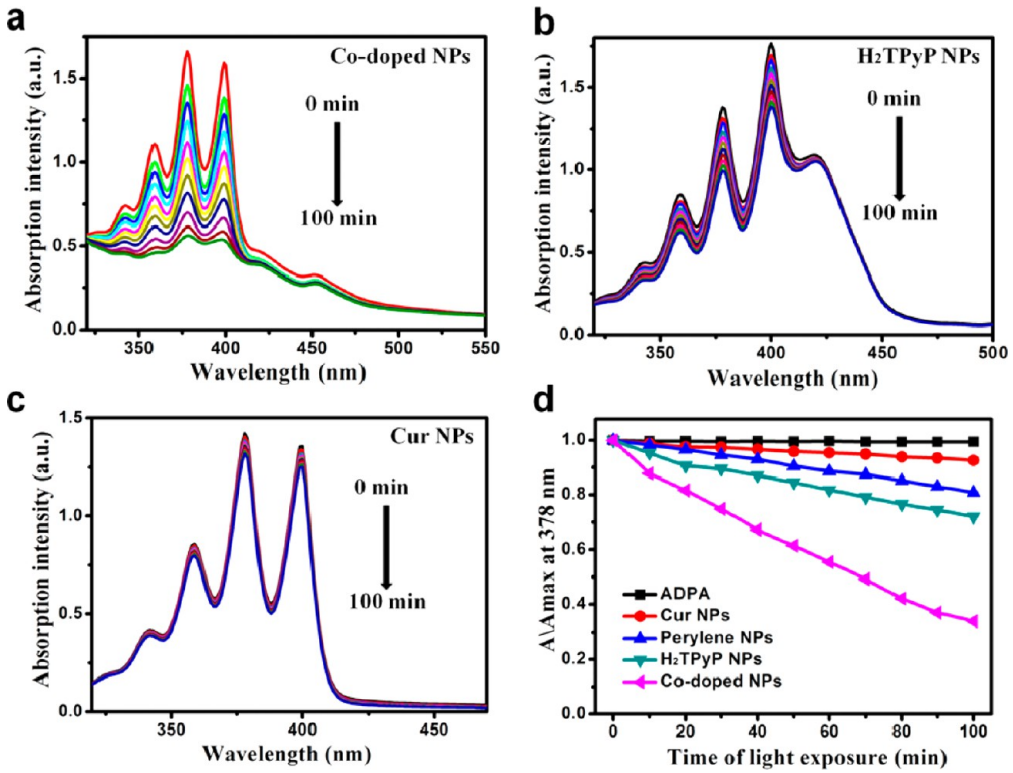

Figure 4. Time-dependent bleaching of ADPA caused by $^1O_2$ generated by (a) the co-doped NPs, (b) the H_2TPyP NPs, and (c) the Cur NPs. (d) The change in ADPA absorption at 378 nm as a function of the irradiation duration.

the $^1O_2$ quantum yield of the pure H_2TPyP NPs and the co-doped NPs solutions are determined to be 3.43% and 10.6%, respectively. The enhanced singlet oxygen generation from the co-doped NPs is due to doping and FRET effects. Both the doping of H_2TPyP into Cur matrix and the FRET effect between H_2TPyP and perylene can significantly improve the $^1O_2$ generation.

Stability. Stability of the nanomaterials in physiological environments is of vital importance prior to their biomedical applications. So herein we measured the stabilities of the co-doped NPs in different conditions as shown in Figure 5. For the intended applications, efficiency of the NPs could be affected by several issues. The first concern is the potential of premature leakage of the photosensitizer before reaching the targeted tissue. Another is the photostability of the photosensitizer. To examine these two potential issues simultaneously, we monitored the absorbance of the co-doped NPs upon irradiation. As depicted in Figure 5a, there is little denaturation after 60 min irradiation. These results indicated that the hydrophobic H_2TPyP molecules are tightly and stably held within the co-doped NPs and do not leak into the aqueous solution under our experimental conditions. Meanwhile, the absorbance of co-doped NPs retains more than 90% of the original intensity after continuously irradiating for 60 min while the absorbance of a commercial organic dye (fluorescein sodium) was decreased to 14% (Figure 5b and Figure S5), which suggested that the co-doped NPs have negligible degradation upon the irradiation.

To further verify the effectiveness of the co-doped NPs to act as an optical imaging agent in a biological environment, the stability of co-doped NPs in different pH conditions was further investigated. As shown in Figure 5c and Figure S6, no obvious fluorescence quenching on the corresponding fluorescence peak (655 nm) was observed in both PBS (pH 7.4) and various buffer solutions with different pH values ranging from 2 to 10 compared with that in pure water, demonstrating that the fluorescence intensity is independent of pH in a wide range, which is beneficial for their potential bioimaging applications. We also measured the monodispersed stability of the co-doped NPs in the aqueous environment to ensure that the co-doped NPs would not aggregate after a period of time. As displayed in Figure 5d, the increase in diameter of the co-doped NPs was negligible in PBS buffer and their PDI value remains around 0.2 within 172 h. Apart from PBS buffer, we also tested the size stability of the co-doped NPs in Dulbecco's modified Eagle's medium (DMEM) supplemented with 10% FBS and 1% penicillin/streptomycin. As shown in Figure S7, the co-doped NPs exhibited good monodispersed stability over 14 days which is essential for further *in vivo* administration. All these results demonstrated that the present co-doped NPs possess good water dispersibility and robust stability in a variety of bioenvironments for further application.

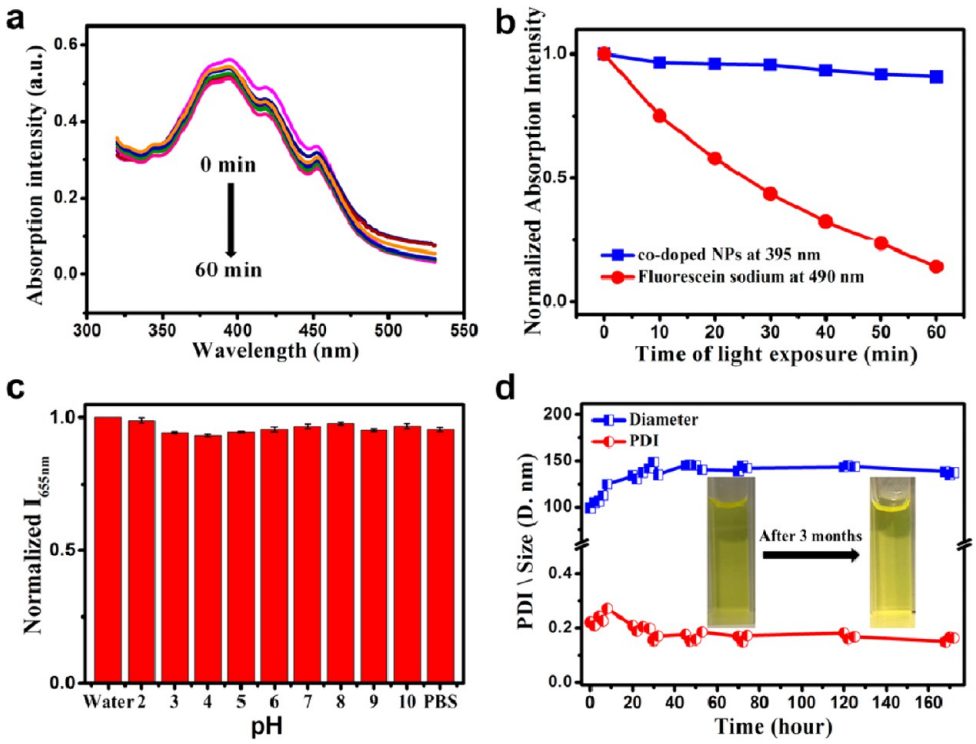

Figure 5. (a,b) Photo- and (c) pH-stabilities of the co-doped NPs. (d) Size-stability of the co-doped NPs dispersed in PBS buffer over 172 h, insets are digital images of the co-doped NPs before (left) and storage (right) for 3 months. Data are the mean ± SD from three separate experiments in Figure 5c.

Cellular Location and Imaging both *in Vitro* and *in Vivo*. Applications of the co-doped NPs for imaging both *in vitro* and *in vivo* were investigated with confocal fluorescence microscopy. A549 cells were individually incubated with the Cur NPs and the co-doped NPs at 37 °C for 4 h. Then fluorescence images were taken with 4,6-diamidino-2-phenylindole (DAPI) as a nucleus located dye. As presented in Figure 6, intense homogeneous cytoplasmic green fluorescence around nuclei can be clearly observed after culture with both the Cur NPs and the co-doped NPs, indicating the release and accumulation of Cur molecules in the cells. Red fluorescence from H_2TPyP can also be seen around the nuclei of the cells cultured with the co-doped NPs (Figure 6c2), confirming the accumulation of H_2TPyP. The inset in Figure 6d2 shows the intracellular redistribution of Cur and H_2TPyP after their release in an A549 cell where the green and red signals could be separately monitored. These results demonstrate that the co-doped NPs can be used as a dual-color fluorescence probe for cell imaging and in intracellular drug trafficking of both Cur and H_2TPyP without using any extra fluorescent dyes.

Inspired by Shi's group who chose zebrafish as an *in vivo* model for optical monitoring,[56] here, we demonstrated dual-color imaging applications of the co-doped NPs in this platform. In our experiment, zebrafish embryos were simply fed with the co-doped or the Cur NPs and monitored with fluorescence imaging after 24 h (Figure 7). Zebrafish embryos fed

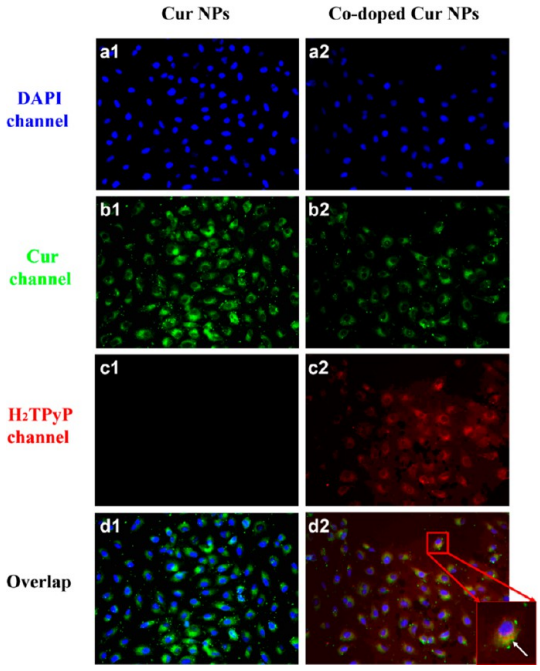

Figure 6. *In vitro* cell imaging and subcellular localization of the Cur NPs (left column) and the co-doped NPs (right column), monitored by fluorescence imaging in A549 cell. (a) DAPI channel; (b) Cur channel; (c) H_2TPyP channel; (d) overlap of the above images. Inset in d2 is a single A549 cell imaging. The white arrow shows redistribution of Cur (green) and H_2TPyP (red).

with the Cur NPs showed only green fluorescence, confirming the release of Cur in the *in vivo* model.

In comparison, both green and red emissions from respectively Cur and H_2TPyP can be detected in around hearts of the zebrafish fed with the co-doped NPs. These results demonstrate the applications of the co-doped NPs for independent tracking of two drugs via the dual-color fluorescence, which are in accordance with the results of *in vitro* evaluations.

Real-Time Self-Monitoring Release of Dual Drugs by Colorimetric Fluorescence Signals. To investigate the change in OFF–ON signal of the Cur and the FRET signals of H_2TPyP following uptake in real-time, the co-doped NPs are incubated with A549 cells. Changes in the Cur and the H_2TPyP signals are measured using confocal fluorescence microscopy with a 405 nm excitation. As displays in Figure 8a, at 0.5 h, only intense red color can be clearly observed in the perinuclear region of the A549 cells, corresponding to the FRET signal from perylene to H_2TPyP. At this stage, the Cur is mostly in the form of NPs which show extremely weak green fluorescence, corresponding to the "OFF" state. With the time increasing to 8 h, a substantial increase of green fluorescence (ON) is observed and is accompanied by a decrease of the red fluorescence intensity. The Cur drug molecules will be sustainedly released through dissolution from the co-doped NP matrix. This self-delivery nanodrug possesses a high loading of Cur in the co-doped NPs, which is essential to preserve the effective drug concentration for sustained and stable drug release.[57,58] The increase in the green fluorescence is consistent with the aforementioned fluorescence spectra of Cur (Figure 2d), as more and more Cur molecules are released leading to the recovery of the green fluorescence from the "OFF" state to "ON" state. In the meantime, the red fluorescence decreases over time due to the release of FRET molecules which increases the distance from donor to acceptor, thus reducing the FRET effect. The overlay images revealing that the fluorescence signals changes from red to orange, then yellow, and finally to yellowish-green can be used for monitoring the release of individual therapeutic agents in real-time. Corresponding flow cytometry studies verified this observation by

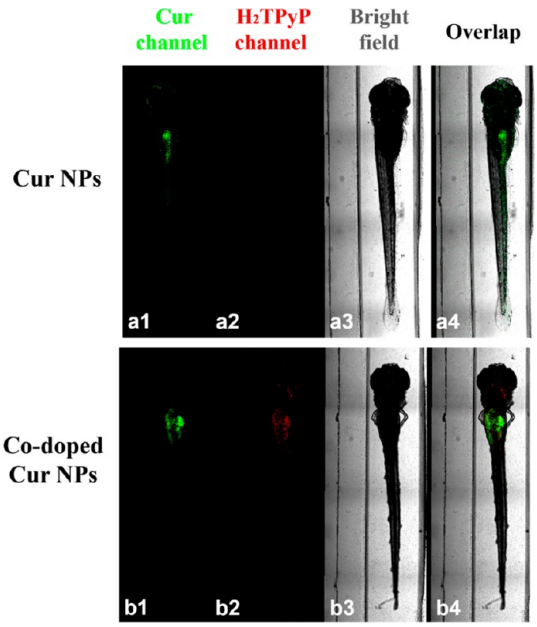

Figure 7. *In vivo* **zebrafish imaging of Cur NPs (left) and co-doped NPs (right). (a) Cur channel; (b) H_2TPyP channel; (c) bright field channel; (d) overlap of the above images.**

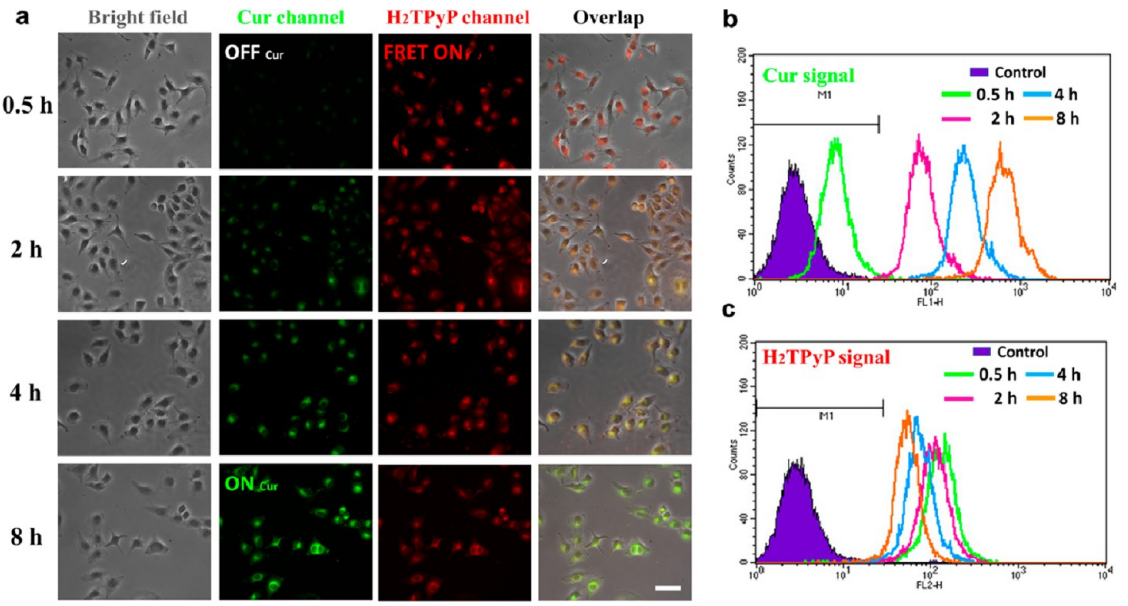

Figure 8. *In vitro* **real-time self-monitoring release of dual drugs. (a) Confocal microscopy images showing changes in the signal of Cur and the FRET signal of H_2TPyP in A549 cells treated with the co-doped NPs at 0.5, 2, 4, and 8 h. Different imaging channels are displayed horizontally for each sample (from left to right): bright field, Cur channel (520–570 nm), H_2TPyP channel (620–670 nm), and overlap images. Scale bar is 25 μm. (b,c) Respectively** *in vitro* **flow cytometry analysis of the fluorescent intensities of Cur and H_2TPyP in A549 cells at 0.5, 2, 4, and 8 h.**

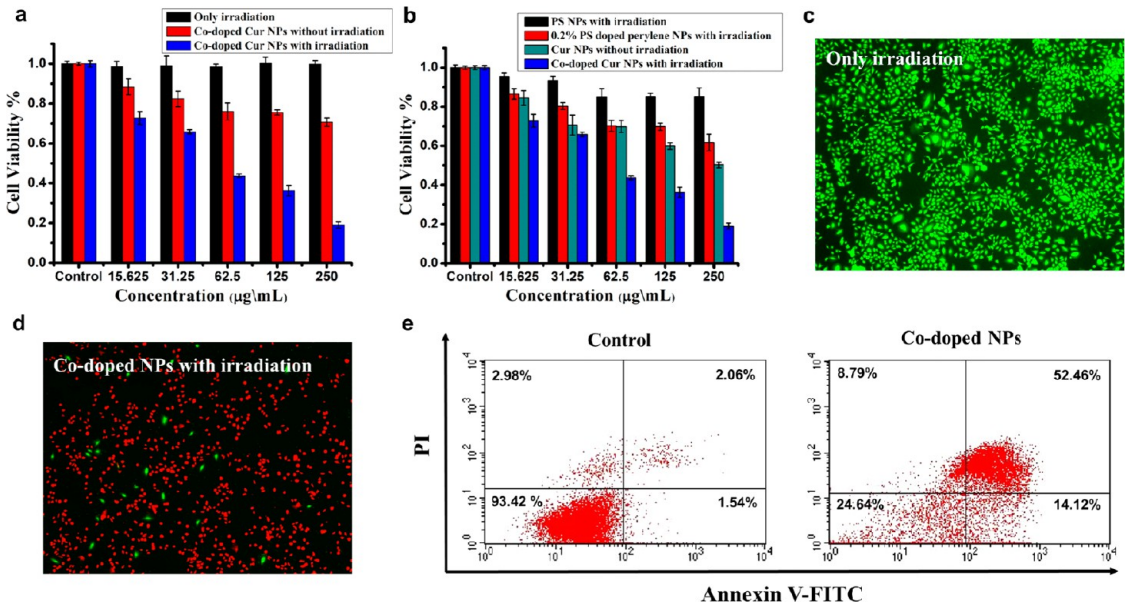

Figure 9. *In vitro* **cytotoxicity. (a) Cytotoxic effects of only irradiation, co-doped NPs without irradiation, co-doped NPs with irradiation against A549 cells with increasing NPs concentrations. (b) Cytotoxic effects of pure H_2TPyP NPs with irradiation, 0.2% H_2TPyP doped perylene NPs (i.e., without Cur) with irradiation, only Cur NPs, the co-doped NPs with irradiation against A549 cells with increasing NPs concentrations. Confocal fluorescence images of calcein AM (green, live cells) and propidium iodide (red, dead cells) costained A549 cells with (c) only irradiation and (d) co-doped NPs with irradiation. (e) Apoptosis and necrosis ratio of A549 cells after treatment with the co-doped NPs with irradiation analyzed using flow cytometry with Annexin V-FITC and PI staining. The quadrants from lower left to upper left (counter clockwise) represent healthy, early apoptotic, late apoptotic, and necrotic cells, respectively. The percentage of cells in each quadrant was shown on the graphs.**

showing an increased Cur fluorescence (Figure 8b) and decreased H_2TPyP fluorescence (Figure 8c) when the co-doped NPs were used. The control experiment in the A549 cells incubated with the H_2TPyP-doped Cur NPs (*i.e.*, without perylene) show a much weaker H_2TPyP signal because of the absence of FRET donor (Figure S8), while the OFF−ON signal of Cur is still clearly observed. Quantitative data in flow cytometry analysis are shown in Table S2 which is in accord with the intensity of the Cur and H_2TPyP signal in Figure 8. Figure S9 further confirmed changes in fluorescence of the co-doped NPs upon release of the Cur molecules. Sample "a" in Figure S9 is DMEM supplemented with 10% FBS and 1% penicillin/streptomycin at 37 °C. Sample "b" was obtained after immediate dispersion of the co-doped NPs (60 μg/mL) into another sample of "a". Sample "c" was obtained by shaking another sample of "b" for 24 h at 37 °C. Under room light, the colors of the three samples are dominated by the color of the DMEM solution (left panel of Figure S9). Upon UV irradiation, sample "a" shows a blue fluorescence, while sample "b" shows an obvious red emission from H_2TPyP. After being shaken for 24 h at 37 °C, sample "c" shows a clear greenish emission. This is consistent with the observation in Figure 8 that green fluorescence from Cur is turned on upon their release from the co-doped NPs.

All these results confirm that the co-doped NPs can be applied as a time-dependent self-monitoring platform for tracking the release profiles of both drugs. Moreover, to evaluate the cytotoxicity of the co-doped NPs for dual color imaging, we measured viability of A549 cells incubated with the co-doped NPs (20 μg/mL) for 0.5, 2, 4, and 8 h, respectively, by MTT assay. As presented in Figure S10, the results confirm that the co-doped NPs exhibit negligible cytotoxicity with A549 cancer cells for different imaging durations.

***In Vitro* Cytotoxicity.** To evaluate the combinatorial therapeutic efficiency of the co-doped NPs, we measured the viability of treated A549 cell lines using 3-(4,5-dimethylthiazol-2-yl)-2,5-diphenyltetrazolium bromide (MTT) assay. A549 cells were individually incubated for 24 h with the co-doped NPs (with or without irradiation), the Cur NPs (without irradiation), the H_2TPyP NPs (with irradiation), and the H_2TPyP/perylene NPs (0.2%) (with irradiation). The control group is the cells with only irradiation but without any NPs. As presented in Figure 9a, both the co-doped NPs with or without irradiation show dose-dependent toxicity while only the irradiation control group exhibits no toxicity. This suggests that the irradiation itself exhibits no cytotoxicity. The co-doped NPs have much higher cytotoxic efficacy upon irradiation as a consequence of the generation of $^1O_2$ from the released H_2TPyP, which leads to reactions with tumor cells and subsequent killing of them by chemical oxidation. It is worth mentioning that a dose-dependent toxicity is also observed in the group of the co-doped NPs in dark conditions. It means that the released chemotherapeutic drug Cur molecules in the co-doped NPs can also kill tumor cells.

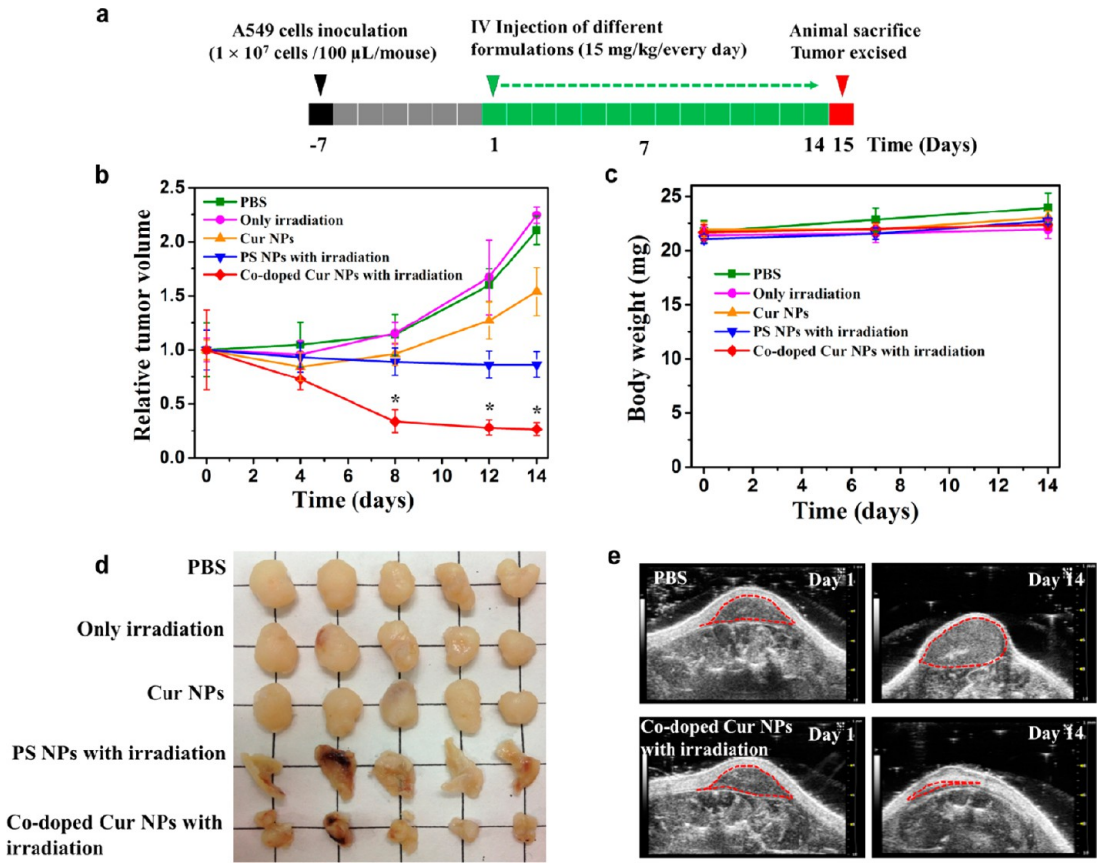

Figure 10. *In vivo* **antitumor activity of the co-doped NPs on A549 Subcutaneous Xenograft Model. (a) A schematic diagram of the experimental design of antitumor effect by using lung cancer xenograft system; (b) rRelative tumor volume in the five mice groups (days 0−14); (c) body weight of mice (days 0−14); (d) images of excised tumors at the time of sacrifice from the subcutaneous A549 lung adenocarcinoma xenograft-bearing male nude mice after 14 days of treatments; (e) comparison of representative ultrasound images of A549 lung tumor xenograft before and after treatment with PBS and the co-doped NPs with irradiation, respectively. Areas marked with red lines are tumor regions determined by performing tumor volume measurements. One-way ANOVA was used to analyze significance of differences (*, $P < 0.05$).**

Furthermore, cytotoxicity from a combination of chemotherapy and PDT was also investigated. In our previous work, we successfully developed 0.2% H_2TPyP-doped perylene NPs for simultaneous enhanced diagnosis and PDT via reducing the aggregation of the H_2TPyP.[53] In this study, we compared the co-doped NPs upon irradiation for combinatorial photochemotherapy with the pure Cur NPs for chemotherapy alone as well as the H_2TPyP and the H_2TPyP/perylene NPs for PDT alone. It has to be pointed out that while perylene does not directly provide any therapeutic effect itself, its presence significantly enhances the singlet oxygen yield via the FRET effects, resulting in much improved therapeutic efficacy.[53] As depicted in Figure 9b, A549 cells exhibit the lowest cell viabilities upon light irradiation in the presence of the co-doped NPs. Particularly, along with the increase of concentration (250 μg\mL), a significant inhibition (up to 81%) of cell growth and proliferation is observed, which is much more effective than in other groups. For example, the cell inhibition efficiency is 49.7% for the pure Cur NPs and only 14.7% for the H_2TPyP at this concentration, respectively. These results confirm that the as-prepared carrier-free co-doped NPs are capable of delivering both Cur and H_2TPyP molecules into cancer cells, leading to remarkably enhanced efficiency in killing cancer cells compared with individual conventional chemotherapy or PDT thatb uses Cur and H_2TPyP alone, respectively.

To further demonstrate the highly effective *in vitro* cytotoxicity of the co-doped NPs, viability of the A549 cells was measured by costaining the cells with calcein acetoxymethylester (Calcine AM) and propidium iodide (PI) to differentiate live (green) and dead (red) cells. The costained cells were irradiated without and with the co-doped NPs. It can be seen that the cells show no observable cytotoxicity upon only irradiation (Figure 9c); while the cells incubated with the co-doped NPs were mostly killed upon the combine actions of the chemotherapeutic drug Cur and the photosensitizer H_2TPyP (Figure 9d). These results are consistent with the MTT results and show that the carrier-free co-doped NPs have a remarkable cell-killing ability, making it a promising platform for cancer therapy.

To investigate the cell death mechanism of the co-doped NPs, A549 cells were double-labeled with

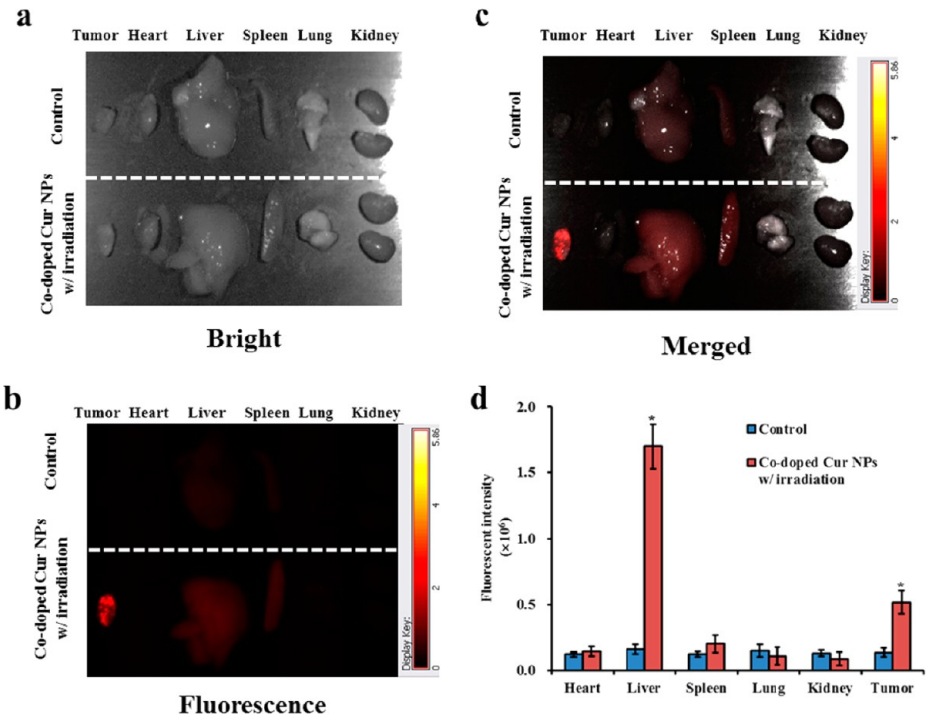

Figure 11. ***In vivo*** **distribution of the co-doped NPs. (a−c)** ***Ex vivo*** **images of the co-doped NPs treated to A549 xenografts. (a) Bright field images; (b) fluorescence images; (c) merged images of major organs and tumor at the time of sacrifice from the subcutaneous A549 lung adenocarcinoma xenograft-bearing male nude mice after 14 days of the co-doped NPs or PBS treatments; (d) quantification of fluorescence intensity of each organ from the co-doped NPs or PBS treated groups. One-way ANOVA was used to analyze significance of differences (∗,** $P < 0.05$**).**

Annexin V-FITC (fluoresceine isothiocyanate) and PI (propidium iodide) before analysis by flow cytometry. The cell populations at different phases of cell death, namely, live (AnnexinV-FITC$^-$/PI$^-$), early apoptotic (Annexin V-FITC$^+$/ PI$^-$), late-stage apoptotic (Annexin V-FITC$^+$/PI$^+$), and necrotic (Annexin V-FITC$^-$/PI$^+$) cells at different treatments are shown in Figure 9e. A mild increase in necrotic of the co-doped NPs with 5 min irradiation treated A549 cells (8.79%) is found compared with the control cells (2.98%), while the percentage of total apoptotic cells (including early and late apoptosis) dramatically increased to 66.58% which is much more than that in the control group (3.6%). Many apoptotic cells could be observed when the cells are treated with the co-doped NPs with irradiation, indicating the strong cytotoxicity of the combination treatment. The above results suggested that the as-designed co-doped NPs with irradiation were a potent and effective strategy to accelerate the apoptosis and necrosis of A549 cells.

In Vivo **Antitumor Activity on A549 Subcutaneous Xenograft Model.** To investigate whether the co-doped NPs do have highly effective therapeutic efficacy *in vivo*, their antitumor activity was assessed on A549 tumor-bearing nude mice. The experimental strategy is presented in a schematic in Figure 10a. A549 cells were subcutaneously injected 7 days before commencing treatment (gray boxes). These animals then received daily intravenous injections of various formulations (green boxes) for 14 days. Cur NPs was administered at an equivalent dose of 15 mg/kg. At day 15, all test mice were sacrificed and corresponding tumors were excised for further studies. During treatment, an LED light source was employed for irradiation purpose (Figure S11). From day 1 to 14, the mice were treated intravenously with PBS, only irradiation, the Cur NPs only, the PS NPs with irradiation, and the co-doped NPs with irradiation, respectively. As shown in Figure 10b, at the end of the experiments, only the co-doped NPs with irradiation group showed a significant tumor regression with a reduction in tumor volume by ∼74%. Mice in the other four groups showed no or mild tumor growth inhibition comparing with the co-doped NPs group. These results confirm that therapeutic efficacy of the combination therapy based on the co-doped NPs is much better than that of monochemotherapy or mono-PDT. Photographs of the tumors from the sacrificed mice are shown in Figure 10d. It can be seen that the tumor volumes in mice treated with the co-doped NPs with irradiation are much smaller than those treated with other formulations. Figure 10e and Figure S12 compare representative ultrasound images of A549 lung tumor xenograft before and after treatments. In particular, Figure S12 shows that the tumor volume in the mice treated with co-doped NPs and irradiation is much smaller as compared to those in other groups. All these results demonstrate that the present combination

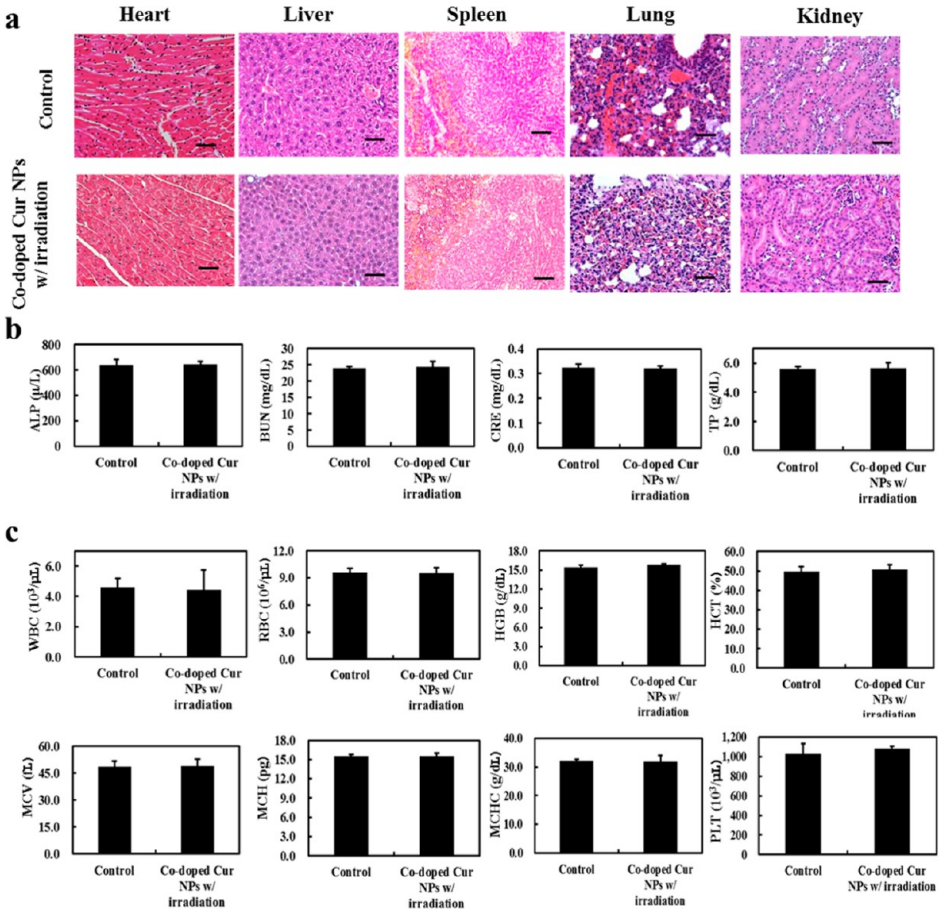

Figure 12. ***In vivo*** **biosafety study of the co-doped NPs. (a) H&E staining images of major organs (heart, liver, spleen, lung, and kidney) of A549 tumor bearing nude mice in groups of PBS and the co-doped NPs with irradiation (scale bar is 50 μm); (b) blood analysis data of the co-doped NPs with irradiation treated. Mice treated with PBS were used as control group. The blood levels of ALP, BUN, CRE, and TP from control and treatment groups. (c) The complete blood panel data from treated mice and control group: WBC, RBC, HGB, MCV, MCH, MCHC, HCT, and PLT. Data are the mean ± SD from three separate experiments.**

therapy does have predominant tumor growth inhibitory efficacy. In addition, no significant weight loss was observed in the tumor-bearing mice treated with various formulations, indicating negligible side effect of the co-doped NPs and light source for tumor therapy at the employed dose (Figure 10c).

In Vivo **Biodistribution and Biosafety.** Next, we evaluated the organ distribution of as-prepared co-doped NPs by using *ex vivo* fluorescence reflectance imaging. After 14 days treatments with the co-doped NPs and PBS buffer, tumor and healthy organs including heart, liver, spleen, lung, and kidney were excised from tumor-bearing mice and scanned *ex vivo*. As shown in Figure 11 panels a−c, an intense red fluorescence can be clearly observed in excised tumor indicating very strong NP accumulation in tumor and less localization in healthy organs. We also quantified the fluorescence intensity of tumor and each organ from the co-doped NPs or PBS treated groups. As presented in Figure11d, the fluorescence intensity of the tumor is higher than that in healthy organs except the liver, which matches the *ex vivo* fluorescence images. The higher level in the liver and spleen reflects that the co-doped NPs are mainly eliminated by macrophage cells of the liver and spleen. As a comparison, the PBS-treated group shows almost the same intensities in tumor and healthy organs. We also measured the pharmacokinetic assay of the co-doped NPs in mice. Mean plasma concentrations of the co-doped NPs in mice after a single intravenous administration of the co-doped NPs were shown in Figure S13. The concentration of the co-doped NPs decreased in plasma 4 h postinjection in a single intravenous administration, so more than a one-time injection of the co-doped NPs formulation is required when carried out for the *in vivo* antitumor activity on the A549 subcutaneous xenograft model.

Potential *in vivo* toxicity has always been a great concern in the development of nanodrugs. Besides measuring body weights of mice in each cohort (Figure 10c), we also collected the hematoxylin and eosin (H&E) staining images of major organs (heart, liver, spleen, lung, and kidney) from A549 tumor-bearing mice in groups of PBS and the co-doped NPs with irradiation, respectively (Figure 12a). Neither noticeable organ damage nor inflammation lesion was

found as compared to the PBS treated group, suggesting no obvious heart, liver, spleen, lung, or kidney dysfunction of mice induced by the co-doped NPs with irradiation treatment. In addition to the H&E staining images, immunohistochemical analysis was also adopted to evaluate the *in vivo* biosafety of the treatments. Age-matched mice treated with PBS were used as a control group. The blood levels of alkaline phosphatase (ALP), blood urea nitrogen (BUN), creatinine (CRE), and total protein (TP) and the complete blood panel data of white blood cells (WBC), red blood cells (RBC), hemoglobin (HGB), mean corpuscular volume (MCV), mean corpuscular hemoglobin (MCH), mean corpuscular hemoglobin concentration (MCHC), hematocrit (HCT), and platelet count (PLT) from treated mice and control group were detected and shown in Figure 12b,c. No observable toxicity was noted in blood analysis. All these results demonstrated that the as-designed co-doped NPs with irradiation show high biosafety for the combination cancer treatment presenting no significant side effects to the treated mice.

CONCLUSIONS

To summarize, for the first time, we successfully developed a self-monitored and self-delivered DDS in combinatorial photochemotherapy against cancer with high drug loading capacity and highly effective theranostic efficacy. Both confocal microscopic images and flow cytometry analysis demonstrated the NPs can be used as a real-time tracking platform. Cell viability studies showed that combined treatment resulted in much higher toxicity than either chemotherapy or PDT alone. Moreover, the co-doped NPs with irradiation exhibit significant inhibition of tumor growth on tumor bearing mice. Besides, this approach (1) addresses the challenge that most PSs are hydrophobic and strongly aggregate in aqueous media by co-doping a pair of FRET donor/acceptor into anticancer a drug Cur matrix, which simultaneously enhanced diagnosis and PDT via doping and FRET; (2) possesses the potential capacity for dual-fluorescent imaging which could simultaneously achieve the self-monitoring of two individual drugs released both *in vitro* and *in vivo*. Both (H&E) staining images and immunohistochemical analysis confirmed the biosafety of the as-designed co-doped NPs with irradiation. Overall, we believe that this highly effective combination cancer theranostic strategy based on carrier-free photosensitizer-doped FRET nanoparticles in the present study may open a new way for combination cancer therapy and diagnosis, and this multiple-therapeutic and multiple-fluorescent agent delivery in a single formulation is of great importance in terms of the advancement of future drug delivery systems.

EXPERIMENTAL SECTION

Materials. Most reagents, including perylene and 5,10,15,20-tetro (4-pyridyl) porphyrin (H_2TPyP), curcumin, 9,10-anthracenedipropionic acid (ADPA), 3-(4,5-dimethylthiazol-2-yl)-2,5-diphenyl tetrazolium bromide (MTT), and THF were purchased from Sigma-Aldrich. Dulbecco's modified Eagle's medium (DMEM), fetal bovine serum (FBS), Dulbecco's phosphate buffered saline (PBS), trypsin-EDTA (0.5% trypsin, 5.3 mM EDTA tetra-sodium), calcein acetoxymethylester (Calcine AM), propidium iodide (PI), and antibiotic agents penicillin–streptomycin were purchased from Life Technologies. Milli-Q water with a resistivity higher than 18.4 MΩ·cm was collected from an in-line Millipore RiOs/Origin water purification system. Unless otherwise noted, all chemicals were obtained from commercial suppliers and used as received.

Preparation of the Co-doped NPs, Cur NPs, and PS NPs. Co-doped NPs were prepared using a reprecipitation method. In a typical procedure, 3 mM solutions of perylene, H_2TPyP, and curcumin in THF were respectively prepared. Samples of 0.6, 299.4, and 700 μL of the H_2TPyP, perylene, and curcumin solutions were then mixed. A 200 μL portion of the mixed solution was quickly dispersed into 5 mL of milli-Q water under vigorous stirring at room temperature for 10 min. Nanoparticles of pristine Cur and H_2TPyP were also prepared with the same procedure.

Characterization of the Co-doped NPs. Size and morphology of the co-doped NPs were investigated using SEM (Philips XL-30 FEG) and TEM (Philips CM200 FEG). The SEM samples were prepared by drying a dispersion of the co-doped NPs on a Si substrate followed by coating of a 2 nm gold layer. The TEM samples were prepared by dripping NPs dispersion onto a holly carbon film followed by drying. DLS measurements were carried out using a Malvern Zetasizer instrument employing a 4 mW He–Ne laser (λ = 632.8 nm) which is equipped with a thermostatic sample chamber.

UV–vis and Fluorescence Measurements. UV–vis spectra were recorded using a Cary 50Conc UV–visible spectrophotometer. Fluorescence spectra were recorded on a Cary Eclipse fluorescence spectrophotometer. Photoirradiation experiments were carried out using a xenon lamp (150 W) equipped with a filter passing light of 400 to 700 nm. High performance liquid chromatography (HPLC) data were obtained on Agilent 1100 gradient system with UV detection at 428 nm.

$^1O_2$ Detection by ADPA. The generation of $^1O_2$ was detected chemically using the disodium salt of ADPA (Sigma) which would be bleached to its corresponding endoperoxide upon contact with $^1O_2$. The reaction was monitored spectrophotometrically by recording the decrease in optical densities at 378 nm. A solution of ADPA (80 μL) in milli-Q water (1 mg/mL) was mixed with 3 mL of different NP dispersions (0.03 mmol/mL). Control samples were preparing by dispersing respectively Cur NPs, H_2TPyP NPs, perylene NPs, and disodium salt of ADPA in milli-Q water. The samples were irradiated with a xenon lamp equipped with a filter passing light of 400 to 700 nm, and their optical densities at 378 nm were recorded every 10 min in a UV–vis spectrophotometer.

***In Vitro* Uptake and Cell Imaging.** A549 cells were cultured with DMEM (Invitrogen) supplemented with 10% FBS (Gibco), penicillin (100 μg/mL), and 1% penicillin/streptomycin (Gibco) in 5% CO_2 at 37 °C in a humidified incubator. The cells were trypsinized and resuspended on 60 mm culture plates, and 2 mL of the medium was combined with 1.0 mL cell suspension. The cells were then seeded on 24-well plates, which were then placed in an incubator at 37 °C overnight with 5% CO_2 for 24 h. Pure Cur NPs and the co-doped NP solutions (20 μg/mL) were added to each plate and carefully mixed. The treated cells were returned to the incubator (37 °C, 5% CO_2) for 4 h. After incubation, the plates were washed thoroughly with sterile PBS. Finally, fluorescent images of the cells were recorded with a Nikon ECLIPSE 80i fluorescent microscope. The real-time

imaging was performed using a Leica laser scanning confocal microscope under 405 nm laser excitation, the signal of Cur (520−570 nm) and the FRET signal of H_2TPyP (620−670 nm) were respectively collected after the A549 cells were treated with the co-doped NPs at 0.5, 2, 4, and 8 h.

***In Vivo* Zebrafish Imaging.** Zebrafish maintenance and embryo collection was performed according to standard operating procedures.[59] Briefly, AB strain zebrafish (*Danio rerio*) were maintained under 14 h light/10 h dark cycles, in circulating freshwater aquaria at 28.5 °C. The fish were fed twice daily with decapsulated and freshly hatched brine shrimps (Brine Shrimp Direct, USA). Zebrafish embryos were obtained from the adults that segregated by sex and mated in tanks overnight. Spawning was induced in the next light cycle when the light was turned on. The embryos were collected and washed using standard zebrafish E3 culture medium (5 mmol/L NaCl, 0.33 mmol/L $CaCl_2$, 0.33 mmol/L $MgSO_4 \cdot 7H_2O$, 0.17 mmol/L KCl) at the one-cell to two-cell stage.[60] The embryos were incubated at 28.5 °C. Larvae at 5 days postfertilization (dpf) were incubated with 15 μg/mL Cur NPs or co-doped NPs for 24 h at 28.5 °C. After washing with PBS, fluorescence from each larva was observed and photographed immediately with a Leica confocal fluorescence microscope.

Flow Cytometry. One-color flow cytometry was done to assess the fluorescence enhancement of our probes upon incubation with A549 cells in a humidified incubator at 37 °C under 5% CO_2 atmosphere. Cells were seeded to reach confluency in 35 mm dishes and treated with the co-doped NPs (20 μg/mL), and at designated time intervals, the cells were harvested after trypsinization and centrifugation at 900 rpm for 10 min. Subsequently, the cell pellets were resuspended in 1 mL of 1X PBS, and flow cytometry was done using a BD FACS Calibur flow cytometer from BD Biosciences.

***In vitro* Cytotoxicity by MTT Assay.** The A549 cells were seeded on 96-well plates in DMEM (with 10% FBS, 1% penicillin/streptomycin). After growing overnight, the cells were used for experiments. After removing the original medium in each well, 200 μL of DMEM containing predetermined concentrations of pure Cur NPs, pure PS NPs, 0.2% PS-doped perylene NPs, and co-doped NPs were added to the designated wells. The final concentration of these NPs on each plate ranged from 15.625 to 250 μg\mL. After 12 h of incubation in the dark at 37 °C, the cells incubated with pure PS NPs, 0.2% PS doped perylene NPs, and co-doped NPs were irradiated for 10 min with broadband visible light using a xenon lamp equipped with a filter passing light of 400 to 700 nm. The power at the cell level was 100 mW/cm^2. The plates were then incubated at 37 °C in the dark for another 12 h. Then, the original medium in each well was removed. Subsequently, 180 μL of DMEM (without FBS) and 20 μL of MTT (Invitrogen) stock solution (5 mg/mL in PBS) were added and incubated for 4 h. Then the medium containing MTT was completely removed, followed by the addition of 200 μL of DMSO (Acros) to each well. Cell viabilities were determined by reading the absorbance of the plates at 540 nm using a BioTek Powerwave XS microplate reader. The cells incubated with serum-supplemented medium represent 100% cell survival. Five replicate wells were run for each concentration and light dose.

Calcine AM/PI Test. The A549 cells were respectively cultured in two 35 mm dishes overnight. The cells in one of the dishes were exposed to the co-doped NPs at the concentration of 250 μg/mL in PBS solution. The drug-treated cells were incubated at 37 °C for 12 h in a humidified atmosphere containing 5% CO_2. Then both dishes of cells were irradiated for 10 min. Then the cells were further incubated at 37 °C for another 12 h. After staining with Calcine AM/PI for 20 min and washing with PBS, the two samples of cells were imaged with a confocal fluorescence microscope.

Animal Study. T-cell deficient male nude (nu/nu) mice, 5−6 weeks of age, were purchased from the National Laboratory Animal Center (Taipei, Taiwan) and were housed in a specific pathogen-free room. All experiments involving the mice were carried out in accordance with Academia Sinica Animal Care and Use Committee guideline. The A549 cells were calculated from the cell viability and cell number by trypan blue, resulting in 1×10^7 live cells in 100 μL of Hank's balanced salt solution (HBSS). When the tumors exhibited a mean diameter of 2−4 mm, the mice were randomly divided into five groups, with each group being composed of five mice. The mice were treated intravenously with PBS, irradiation alone, Cur NPs only, H_2TPyP NPs with irradiation, and the co-doped NPs with irradiation, respectively. Cur NPs was administered at an equivalent dose of 15 mg/kg. All tumors were measured every other day with ultrasound imaging system (Vevo 2100, FujiFilm VisualSonics, Inc. Toronto, ON, Canada) during the period of study. After 14 days of drugs administrations, the mice were sacrificed. Tumor volume and weight are expressed as mean ± SD. Statistical significance of differences between treatments was determined by one-way analysis of variance (ANOVA). $P < 0.05$ was considered to statistically significant.

Pharmacokinetic Studies in Mice. The pharmacokientic properties of the co-doped NPs after a single intravenous injection dose were studied in 6-week-old male mice. The co-doped NPs were given by intravenous injection at a dose of 15 mg/kg, and mice were sacrificed at various intervals after administration. Plasma was obtained from blood treated with 1.5 mg/mL K_2EDTA by centrifuge at 3000*g* for 10 min. Plasma sample detection was achieved at 635 nm by Synergy H1Multi-Mode Reader (BioTek Instruments, Inc., Winooski, VT, USA).

***In Vivo* Imaging of Tissue Distribution Studies.** The *in vivo* biodistribution of the co-doped NPs in A549 tumor bearing mice was performed using CRI Maestro animal imaging system (CRI Corporation, Woburn, MA, USA). On the 14th day after drug administration, mice were sacrificed, and major organs including heart, liver, spleen, lung, kidney, and tumor were carefully removed for visualization under the imaging system. The fluorescent signals of each organ were analyzed by the accompanied software.

***In Vivo* Biosafety Studies.** On the 14th day after drug administration, mice were sacrificed and blood samples were collected into tubes containing 1.5 mg/mL K_2EDTA for complete blood cell count. Plasma was separated into cryotubes and store at −80 °C until blood chemistry analysis. Major organs (heart, liver, spleen, lung, and kidney) were dissected for H&E staining.

Conflict of Interest: The authors declare no competing financial interest.

Supporting Information Available: The Supporting Information is available free of charge on the ACS Publications website at DOI: 10.1021/acsnano.5b02513.

Description of materials and methods and Supporting Figures: (Figure S1) standard absorbance curve of Cur, (Figure S2) standard absorbance curve of H_2TPyP, (Figure S3) time-dependent bleaching of ADPA caused by singlet oxygen generated by (a) H_2TPyP NPs and (b) ADPA, (Figure S4) chemical trapping measurements of the $^1O_2$ quantum yield of the H_2TPyP NPs and the co-doped NPs. (Figure S5) Photostabilities of commercial organic dye (fluorescein sodium) dispersed in milli-Q water, (Figure S6) photostabilities of the co-doped NPs in different pH, (Figure S7) size-stability of the co-doped NPs dispersed in DMEM supplemented with 10% FBS and 1% penicillin/streptomycin over 14 days, (Figure S8) confocal microscopy images showing the change in OFF−ON signal of Cur and H_2TPyP in A549 cells treated with just PS-doped Cur NPs without perylene at 0.5, 2, 4, and 8 h, (Figure S9) photographs of the DMEM supplemented with 10% FBS and 1% penicillin/streptomycin., the co-doped NPs incubated in DMEM supplemented with 10% FBS and 1% penicillin/streptomycin for 5 min, the co-doped NPs incubated in DMEM supplemented with 10% FBS and 1% penicillin/streptomycin for 24 h under room light (left photos) and UV light (right photos), (Figure S10) *in vitro* cytotoxicity of the co-doped NPs incubated in A549 cells for 0.5, 2, 4, and 8 h respectively, (Figure S11) LED light instrument used for irradiation during the treatment. (Figure S12) Comparison of representative ultrasound images of A549 lung tumor xenograft before and after treatment with PBS and the co-doped NPs with irradiation, respectively, (Figure S13) pharmacokinetic assay of the co-doped NPs in mice. Mean plasma concentrations of the co-doped NPs in mice after

single intravenous administration of the co-doped NPs. (Table S1) Comparison of drug loading content (wt %) between our carrier-free co-doped NPs and other carrier-based drug delivery system for combinatorial therapy. (Table S2) Quantitative data in flow cytometry analysis with time increasing from 0.5 to 8 h (PDF)

Acknowledgment. The authors thank the Laboratory Animal Core Facility funded by the Agriculture Biotechnology Research Center (ABRC) at Academia Sinica, Taiwan, for animal vivarium and technical support. The authors also acknowledge Dr. Andrei Susha and Dr. Stephen V. Kershaw for providing research support in Hong Kong Science Park. This work was supported in part by UST-UCSD International Center of Excellence in Advanced Bioengineering sponsored by the Ministry of Science and Technology I-RiCE Program under Grant Number MOST 103-2911-I-009-101.

REFERENCES AND NOTES

1. Peer, D.; Karp, J. M.; Hong, S.; Farokhzad, O. C.; Margalit, R.; Langer, R. Nanocarriers as an Emerging Platform for Cancer Therapy. *Nat. Nanotechnol.* **2007**, *2*, 751–760.
2. Irvine, D. J. Drug delivery: One Nanoparticle, One Kill. *Nat. Mater.* **2011**, *10*, 342–343.
3. Hubbell, J. A.; Langer, R. Translating Materials Design to the Clinic. *Nat. Mater.* **2013**, *12*, 963–966.
4. Mura, S.; Nicolas, J.; Couvreur, P. Stimuli-Responsive Nanocarriers for Drug Delivery. *Nat. Mater.* **2013**, *12*, 991–1003.
5. Cafeo, G.; Carbotti, G.; Cuzzola, A.; Fabbi, M.; Ferrini, S.; Kohnke, F. H.; Papanikolaou, G.; Plutino, M. R.; Rosano, C.; White, A. J. P. Drug Delivery with a Calixpyrrole−trans-Pt (II) Complex. *J. Am. Chem. Soc.* **2013**, *135*, 2544–2551.
6. Wu, X.; Sun, X.; Guo, Z.; Tang, J.; Shen, Y.; Tian, H.; Zhu, W.; James, T. D. In Vivo and In Situ Tracking Cancer Chemotherapy by Highly Photostable NIR Fluorescent Theranostic Prodrug. *J. Am. Chem. Soc.* **2014**, *136*, 3579–3588.
7. Liang, X.; Li, X.; Yue, X.; Dai, Z. Conjugation of Porphyrin to Nanohybrid Cerasomes for Photodynamic Diagnosis and Therapy of Cancer. *Angew. Chem., Int. Ed.* **2011**, *50*, 11622–11627.
8. Idris, N. M.; Gnanasammandhan, M. K.; Zhang, J.; Ho, P. C.; Mahendran, R.; Zhang, Y. In Vivo Photodynamic Therapy Using Upconversion Nanoparticles as Remote-Controlled Nanotransducers. *Nat. Med.* **2012**, *18*, 1580–1585.
9. Cheng, L.; He, W.; Gong, H.; Wang, C.; Chen, Q.; Cheng, Z.; Liu, Z. PEGylated Micelle Nanoparticles Encapsulating a Non-Fluorescent Near-Infrared Organic Dye as a Safe and Highly-Effective Photothermal Agent for In Vivo Cancer Therapy. *Adv. Funct. Mater.* **2013**, *23*, 5893–5902.
10. Ge, J.; Lan, M.; Zhou, B.; Liu, W.; Guo, L.; Wang, H.; Jia, Q.; Niu, G.; Huang, X.; Zhou, H.; et al. A Graphene Quantum Dot Photodynamic Therapy Agent with High Singlet Oxygen Generation. *Nat. Commun.* **2014**, 10.1038/ncomms5596.
11. Dolmans, D. E. J. G. J.; Fukumura, D.; Jain, R. K. Photodynamic Therapy for Cancer. *Nat. Rev. Cancer* **2003**, *3*, 380–387.
12. Lovell, J. F.; Liu, T. W. B.; Chen, J.; Zheng, G. Activatable Photosensitizers for Imaging and Therapy. *Chem. Rev.* **2010**, *110*, 2839–2857.
13. Zheng, M.; Yue, C.; Ma, Y.; Gong, P.; Zhao, P.; Zheng, C.; Sheng, Z.; Zhang, P.; Wang, Z.; Cai, L. Single-Step Assembly of DOX/ICG Loaded Lipid-Polymer Nanoparticles for Highly Effective Chemo-photothermal Combination Therapy. *ACS Nano* **2013**, *7*, 2056–2067.
14. Mauceri, H. J.; Hanna, N. N.; Beckett, M. A.; Gorski, D. H.; Staba, M. J.; Stellato, K. A.; Bigelow, K.; Heimann, R.; Gately, S.; Dhanabal, M.; et al. Combined Effects of Angiostatin and Ionizing Radiation in Antitumour Therapy. *Nature* **1998**, *394*, 287–291.
15. Lane, D. Designer Combination Therapy for Cancer. *Nat. Biotechnol.* **2006**, *24*, 163–164.
16. Barick, K. C.; Singh, S.; Jadhav, N. V.; Bahadur, D.; Pandey, B. N.; Hassan, P. A. pH-Responsive Peptide Mimic Shell Cross-Linked Magnetic Nanocarriers for Combination Therapy. *Adv. Funct. Mater.* **2012**, *22*, 4975–4984.
17. Dong, K.; Liu, Z.; Li, Z.; Ren, J.; Qu, X. Hydrophobic Anticancer Drug Delivery by a 980 nm Laser-Driven Photothermal Vehicle for Efficient Synergistic Therapy of Cancer Cells In Vivo. *Adv. Mater.* **2013**, *25*, 4452–4458.
18. Li, W.; Liao, P.; Su, C.; Yeh, C. Formation of Oligonucleotide-Gated Silica Shell-Coated Fe3O4-Au Core−Shell Nanotrisoctahedra for Magnetically Targeted and Near-Infrared Light-Responsive Theranostic Platform. *J. Am. Chem. Soc.* **2014**, *136*, 10062–10075.
19. Topete, A.; Alatorre-Meda, M.; Iglesias, P.; Villar-Alvarez, E. M.; Barbosa, S.; Costoya, J. A.; Taboada, P.; Mosquera, V. Fluorescent Drug-Loaded, Polymeric-Based, Branched Gold Nanoshells for Localized Multimodal Therapy and Imaging of Tumoral Cells. *ACS Nano* **2014**, *8*, 2725–2738.
20. Li, N.; Yang, H.; Pan, W.; Diao, W.; Tang, B. A Tumour mRNA-Triggered Nanocarrier for Multimodal Cancer Cell Imaging and Therapy. *Chem. Commun.* **2014**, *50*, 7473–7476.
21. You, J.; Guo, P.; Auguste, D. T. A Drug-Delivery Vehicle Combining the Targeting and Thermal Ablation of HER^{2+} Breast-Cancer Cells with Triggered Drug Release. *Angew. Chem., Int. Ed.* **2013**, *52*, 4141–4146.
22. Wang, L.; Lin, X.; Wang, J.; Hu, Z.; Ji, Y.; Hou, S.; Zhao, Y.; Wu, X.; Chen, C. Novel Insights into Combating Cancer Chemotherapy Resistance Using a Plasmonic Nanocarrier: Enhancing Drug Sensitiveness and Accumulation Simultaneously with Localized Mild Photothermal Stimulus of Femtosecond Pulsed Laser. *Adv. Funct. Mater.* **2014**, *24*, 4229–4239.
23. Liu, T.; Wang, C.; Gu, X.; Gong, H.; Cheng, L.; Shi, X.; Feng, L.; Sun, B.; Liu, Z. Drug Delivery with PEGylated MoS_2 Nanosheets for Combined Photothermal and Chemotherapy of Cancer. *Adv. Mater.* **2014**, *26*, 3433–3440.
24. Zhang, Z.; Wang, J.; Nie, X.; Wen, T.; Ji, Y.; Wu, X.; Zhao, Y.; Chen, C. Near Infrared Laser-Induced Targeted Cancer Therapy Using Thermoresponsive Polymer Encapsulated Gold Nanorods. *J. Am. Chem. Soc.* **2014**, *136*, 7317–7326.
25. Gong, H.; Dong, Z.; Liu, Y.; Yin, S.; Cheng, L.; Xi, W.; Xiang, J.; Liu, K.; Li, Y.; Liu, Z. Engineering of Multifunctional Nano-Micelles for Combined Photothermal and Photodynamic Therapy under the Guidance of Multimodal Imaging. *Adv. Funct. Mater.* **2014**, *24*, 6492–6502.
26. Topete, A.; Alatorre-Meda, M.; Iglesias, P.; Villar-Alvarez, E. M.; Barbosa, S.; Costoya, J. A.; Taboada, P.; Mosquera, V. Fluorescent Drug-Loaded, Polymeric-Based, Branched Gold Nanoshells for Localized Multimodal Therapy and Imaging of Tumoral Cells. *ACS Nano* **2014**, *8*, 2725–2738.
27. Son, K. J.; Yoon, H.; Kim, J.; Jang, W.; Lee, Y.; Koh, W. Photosensitizing Hollow Nanocapsules for Combination Cancer Therapy. *Angew. Chem., Int. Ed.* **2011**, *50*, 11968–11971.
28. Miao, W.; Shim, G.; Lee, S.; Lee, S.; Choe, Y. S.; Oh, Y. Safety and Tumor Tissue Accumulation of PEGylated Graphene Oxide Nanosheets for Co-Delivery of Anticancer Drug and Photosensitizer. *Biomaterials* **2013**, *34*, 3402–3410.
29. Pasparakis, G.; Manouras, T.; Vamvakaki, M.; Argitis, P. Harnessing Photochemical Internalization with Dual Degradable Nanoparticles for Combinatorial Photo-Chemotherapy. *Nat. Commun.* **2014**, *47*, 3052–3060.
30. Croissant, J.; Salles, D.; Maynadier, M.; Mongin, O.; Hugues, V.; Blanchard-Desce, M.; Cattoën, X.; Chi, M. W.; Gallud, A.; Garcia, M.; et al. Mixed Periodic Mesoporous Organosilica Nanoparticles and Core-Shell Systems, Application to in Vitro Two-Photon Imaging, Therapy, and Drug Delivery. *Chem. Mater.* **2014**, *26*, 7214–7220.
31. Deng, X.; Liang, Y.; Peng, X.; Su, T.; Luo, S.; Cao, J.; Gu, Z.; He, B. A Facile Strategy to Generate Polymeric Nanoparticles for Synergistic Chemo-Photodynamic Therapy. *Chem. Commun.* **2015**, *51*, 4271–4274.
32. He, C.; Liu, D.; Lin, W. Self-Assembled Core-Shell Nanoparticles for Combined Chemotherapy and Photodynamic Therapy of Resistant Head and Neck Cancers. *ACS Nano* **2015**, *9*, 991–1003.
33. Huang, P.; Wang, D.; Su, Y.; Huang, W.; Zhou, Y.; Cui, D.; Zhu, X.; Yan, D. Combination of Small Molecule Prodrug and

Nanodrug Delivery: Amphiphilic Drug-Drug Conjugate for Cancer Therapy. *J. Am. Chem. Soc.* **2014**, *136*, 11748–11758.
34. Poland, C. A.; Duffin, R.; Kinloch, I.; Maynard, A.; Wallace, W. A. H.; Seaton, A.; Stone, V.; Brown, S.; MacNee, W.; Donaldson, K. Carbon Nanotubes Introduced Into The Abdominal Cavity Of Mice Show Asbestos-Like Pathogenicity in a Pilot Study. *Nat. Nanotechnol.* **2008**, *3*, 423–428.
35. Alkilany, A. M.; Shatanawi, A.; Kurtz, T.; Caldwell, R. B.; Caldwell, R. W. Toxicity and Cellular Uptake of Gold Nanorods in Vascular Endothelium and Smooth Muscles of Isolated Rat Blood Vessel: Importance of Surface Modification. *Small* **2012**, *8*, 1270–1278.
36. Shen, Y.; Jin, E.; Zhang, B.; Murphy, C. J.; Sui, M.; Zhao, J.; Wang, J.; Tang, J.; Fan, M.; Kirk, E. V.; et al. Prodrugs Forming High Drug Loading Multifunctional Nanocapsules for Intracellular Cancer Drug Delivery. *J. Am. Chem. Soc.* **2010**, *132*, 4259–4265.
37. Baba, K.; Pudavar, H. E.; Roy, I.; Ohulchanskyy, T. Y.; Chen, Y.; Pandey, R. K.; Prasad, P. N. New Method for Delivering a Hydrophobic Drug for Photodynamic Therapy Using Pure Nanocrystal Form of the Drug. *Mol. Pharmaceutics* **2007**, *4*, 289–297.
38. Kasai, H.; Murakami, T.; Ikuta, Y.; Koseki, Y.; Baba, K.; Oikawa, H.; Nakanishi, H.; Okada, M.; Shoji, M.; Ueda, M.; et al. Creation of Pure Nanodrugs and Their Anticancer Properties. *Angew. Chem., Int. Ed.* **2012**, *51*, 10315–10319.
39. Li, W.; Zhang, X.; Hao, X.; Jie, J.; Tian, B.; Zhang, X. Shape Design of High Drug Payload Nanoparticles for More Effective Cancer Therapy. *Chem. Commun.* **2013**, *49*, 10989–10991.
40. Tan, X.; Li, B. B.; Lu, X.; Jia, F.; Santori, C.; Menon, P.; Li, H.; Zhang, B.; Zhao, J. J.; Zhang, K. Light-Triggered, Self-Immolative Nucleic Acid-Drug Nanostructures. *J. Am. Chem. Soc.* **2015**, *137*, 6112–6115.
41. Zhang, J.; Li, Y.; An, F. F.; Zhang, X.; Chen, X.; Lee, C. S. Preparation and Size Control of Sub-100 nm Pure Nanodrugs. *Nano Lett.* **2015**, *15*, 313–318.
42. Yu, C.; Zhou, M.; Zhang, X.; Wei, W.; Chen, X.; Zhang, X. Smart doxorubicin nanoparticles with high drug payload for enhanced chemotherapy against drug resistance and cancer diagnosis. *Nanoscale* **2015**, *7*, 5683–5690.
43. Lee, M. H.; Kim, J. Y.; Han, J. H.; Bhuniya, S.; Sessler, J. L.; Kang, C.; Kim, J. S. Direct Fluorescence Monitoring of The Delivery And Cellular Uptake of A Cancer-Targeted RGD Peptide-Appended Naphthalimide Theragnostic Prodrug. *J. Am. Chem. Soc.* **2012**, *134*, 12668–12674.
44. Peng, F.; Su, Y.; Wei, X.; Lu, Y.; Zhou, Y.; Zhong, Y.; Lee, S. T.; He, Y. Silicon-Nanowire-Based Nanocarriers with Ultrahigh Drug-Loading Capacity for *In Vitro* and *In Vivo* Cancer Therapy. *Angew. Chem., Int. Ed.* **2013**, *52*, 1457–1461.
45. Maiti, S.; Park, N.; Han, J. H.; Jeon, H. M.; Lee, J. H.; Bhuniya, S.; Kang, C.; Kim, J. S. Gemcitabine-Coumarin-Biotin Conjugates: A Target Specific Theranostic Anticancer Prodrug. *J. Am. Chem. Soc.* **2013**, *135*, 4567–4572.
46. Xing, Q.; Li, N.; Chen, D.; Sha, W.; Jiao, Y.; Qi, X.; Xu, Q.; Lu, J. Light-Responsive Amphiphilic Copolymer Coated Nanoparticles as Nanocarriers and Real-Time Monitors for Controlled Drug Release. *J. Mater. Chem. B* **2014**, *2*, 1182–1189.
47. Zhang, P.; Cheng, F.; Zhou, R.; Cao, J.; Li, J.; Burda, C.; Min, Q.; Zhu, J. DNA-Hybrid-Gated Multifunctional Mesoporous Silica Nanocarriers for Dual-Targeted and MicroRNA-Responsive Controlled Drug Delivery. *Angew. Chem., Int. Ed.* **2014**, *53*, 2371–2375.
48. Wu, M.; Meng, Q.; Chen, Y.; Xu, P.; Zhang, S.; Li, Y.; Zhang, L.; Wang, M.; Yao, H.; Shi, J. Ultrasmall Confined Iron Oxide Nanoparticle MSNs as a pH-Responsive Theranostic Platform. *Adv. Funct. Mater.* **2014**, *24*, 4273–4283.
49. Sun, T.; Zhang, Y. S.; Pang, B.; Hyun, D. C.; Yang, M.; Xia, Y. Engineered Nanoparticles for Drug Delivery in Cancer Therapy. *Angew. Chem., Int. Ed.* **2014**, *53*, 12320–12364.
50. Tang, H.; Murphy, C. J.; Zhang, B.; Shen, Y.; Kirk, E. A. V.; Murdoch, W. J.; Radosz, M. Curcumin Polymers as Anticancer Conjugates. *Biomaterials* **2010**, *31*, 7139–7149.
51. Rabinow, B. E. Nanosuspensions in drug delivery. *Nat. Rev. Drug Discovery* **2004**, *3*, 785–796.
52. Salazar, J.; Ghanem, A.; Müller, R. H.; Möschwitzer, J. P. Nanocrystals: Comparison of the size reduction effectiveness of a novel combinative method with conventional top-down approaches. *Eur. J. Pharm. Biopharm.* **2012**, *81*, 82–90.
53. Zhang, J.; An, F.; Li, Y.; Zheng, C.; Yang, Y.; Zhang, X.; Zhang, X. Simultaneous Enhanced Diagnosis and Photodynamic Therapy of Photosensitizer-doped Perylene Nanoparticles *via* Doping, Fluorescence Resonance Energy Transfer, and Antenna Effect. *Chem. Commun.* **2013**, *49*, 8072–8074.
54. Krasnovsky, A. A., Jr. Singlet Molecular Oxygen in Photobiochemical Systems: IR Phosphorescence Studies. *Membr. Cell Biol.* **1998**, *12*, 665–690.
55. Lindig, B. A.; Rodgers, M. A. J.; Schaap, A. P. Determination of The Lifetime of Singlet Oxygen in Water-d_2 Using 9, 10-Anthracenedipropionic Acid, A Water-Soluble Probe. *J. Am. Chem. Soc.* **1980**, *102*, 5590–5593.
56. Liu, J.; Bu, J.; Bu, W.; Zhang, S.; Pan, L.; Fan, W.; Chen, F.; Zhou, L.; Peng, W.; Zhao, K.; et al. Real-Time In Vivo Quantitative Monitoring of Drug Release by Dual-Mode Magnetic Resonance and Upconverted Luminescence Imaging. *Angew. Chem., Int. Ed.* **2014**, *53*, 4551–4555.
57. Wang, H.; Yang, Z. Molecular Hydrogels of Hydrophobic Compounds: A Novel Self-Delivery System for Anti-Cancer Drugs. *Soft Matter* **2012**, *8*, 2344–2347.
58. Lin, Z.; Gao, W.; Hu, H.; Ma, K.; He, B.; Dai, W.; Wang, X.; Wang, J.; Zhang, X.; Zhang, Q. Novel Thermo-Sensitive Hydrogel System with Paclitaxel Nanocrystals: High Drug-Loading, Sustained Drug Release and Extended Local Retention Guaranteeing Better Efficacy and Lower Toxicity. *J. Controlled Release* **2014**, *174*, 161–170.
59. Westerfield, M. *The Zebrafish Book. A Guide for the Laboratory Use of Zebrafish (Danio Rerio)*; University of Oregon Press: Corvallis, 2000.
60. Brand, M.; Granato, M.; Nüsslein-Volhard, C. *Keeping and Raising Zebrafish*; Oxford University Press: Oxford, 2002; pp 21−22.